Journal of Sound and Vibration (2002) **252**(1), 19–36
doi:10.1006/jsvi.2001.4022, available online at http://www.idealibrary.com on IDEAL®

ACTIVE CONTROL EXPERIMENTS FOR ACOUSTIC RADIATION REDUCTION OF A SANDWICH PANEL: FEEDBACK AND FEEDFORWARD INVESTIGATIONS

B. Petitjean and I. Legrain

ONERA/DDSS, BP 72, 29 *avenue de la division Leclerc*, 92322 *Châtillon Cedex, France*

and

F. Simon and S. Pauzin

ONERA/DMAE, BP 4025, 31055 *Toulouse Cedex* 04, *France*

(*Received* 29 *September* 2000, *and in final form* 28 *August* 2001)

Experiments were conducted on a square panel of a honeycomb sandwich material, to compare and evaluate various active control strategies for acoustic radiation reduction. The panel was clamped between two soundproofed rooms, the receiving room being equipped with a moving system and a microphone. This paper compares different sensor/actuator arrangements. The two basic configurations are 8 PVDF patches used as sensors on one side of the panel and 8 PZT patches on the other side, versus several accelerometers or microphones as sensors and secondary shakers as actuators. In all cases, the primary excitation is provided by a shaker generating either pure tones or broadband noise on wide frequency bands (0–800 Hz). The second comparison level is relative to the control approaches: LMS feedforward and collocated feedback control strategies are investigated for broadband primary excitations. One of the most interesting aspects of the problem is to evaluate active control methods applied to a highly damped material. In particular, modal analysis and system identification are much more difficult than when applied to lightly damped metallic structures, due to the high modal overlap.

1. INTRODUCTION

Noise reduction in helicopter cabins is one of the major challenges for future rotorcraft programs. Low interior noise levels can indeed be a major competitive advantage, comparable to other performance features.

However, composite materials are becoming more and more widely used in helicopter structures. Unfortunately, this leads to significant degradation of the acoustic comfort in the cabin: the combination of low density, high stiffness and large thickness lowers the critical frequency [1], where the noise transmission is maximum.

Passive approaches to alleviate this problem have been used in the past and are still a strong motivation for research activity [2]. An example of passive optimization is presented in reference [3]. However, these approaches tend to be efficient only in the upper frequency range. Massive use of damping materials usually also leads to a significant mass increase, that the use of composites was designed to avoid.

There is also a potential for *active* noise reduction systems based on control of the structure itself. These active systems are likely to compensate for the lack of efficiency of

0022-460X/02/$35.00

passive methods in the low-frequency domain, and usually add less mass to the overall system. This control approach is termed active structural acoustic control (ASAC), in contrast to active noise control (ANC), where secondary sound sources are used to lower the initial sound field.

There is now a considerable body of literature, including journal articles [4–7], proceedings papers [8, 9] and even textbooks [10, 11], that investigate this control approach. Unfortunately, most of them are limited to *weakly damped metallic structures.* However, it turns out that extending active control strategies to highly damped composite structures is not straightforward:

(1) Composite structures are inherently more difficult to model than their metallic counterparts, not to mention their potential heterogeneities and the differences in dynamic behavior between supposedly identical samples.
(2) The high level of structural damping exhibited by typical composite structures, including sandwich honeycomb panels, adds to the difficulty of dynamic analysis: modal analysis is hampered by the high modal overlap.

This paper addresses these problems, illustrated by the case of a sandwich honeycomb panel consisting of a Nomex core and two fiberglass skins, in the frequency range of 0–800 Hz.

Two main types of disturbances causing a high noise level inside helicopter cabins are encountered. The first type is pure tones due to rotational mechanical elements, such as gearbox mechanisms. The second type is broadband excitations from various sources, including turbulent boundary layer excitation. The hybrid nature of the disturbances calls for a hybrid control architecture (feedforward and feedback), because the usual feedforward algorithms require the use of a reference signal closely correlated with the error signal. This reference signal may be unavailable in the case of stochastic broadband disturbances. This paper investigates both the approaches.

Furthermore, comparisons are given between various sensor/actuator configurations, various excitation spectra, and between the two control approaches, strictly applied to the *same structure*, in the *same environment*. This kind of comparison is relatively new, to the authors' knowledge. Although some papers [12–14] investigate the links between the two worlds, there is still a gap to fill.

This paper is organized as follows: the experimental test set-up is described in the first part, along with the different excitation cases and sensor and actuator sets. The next section is devoted to the theoretical aspects, structural dynamics and control theory. Experimental results are presented and analyzed next, for both feedforward control and feedback control. The final section is focused on the feedback/feedforward comparison.

2. DESCRIPTION OF THE EXPERIMENTAL SET-UP

Experiments were carried out on a Nomex honeycomb/fiberglass panel, clamped in an aperture separating two soundproofed rooms. The panel thickness was 20 mm, its overall dimensions were $0{\cdot}90 \times 0{\cdot}90\,\mathrm{m}^2$. Because of clamping frames, only a smaller area of $0{\cdot}84 \times 0{\cdot}84\,\mathrm{m}^2$ was actually vibrating.

The primary excitation (representing the perturbation) was provided by a dynamic shaker whose position allows excitation of many modes. The secondary actuators (providing the control input) were either three additional dynamic shakers (four tested locations) or a set of eight PZT (lead titanate/zirconate) patches bonded on the panel surface. The patches measured $80 \times 50 \times 1\,\mathrm{mm}^3$. Figure 1 shows the equipped panel. Optimal placement of the PZT patches was based on a method outlined in section 3.1.

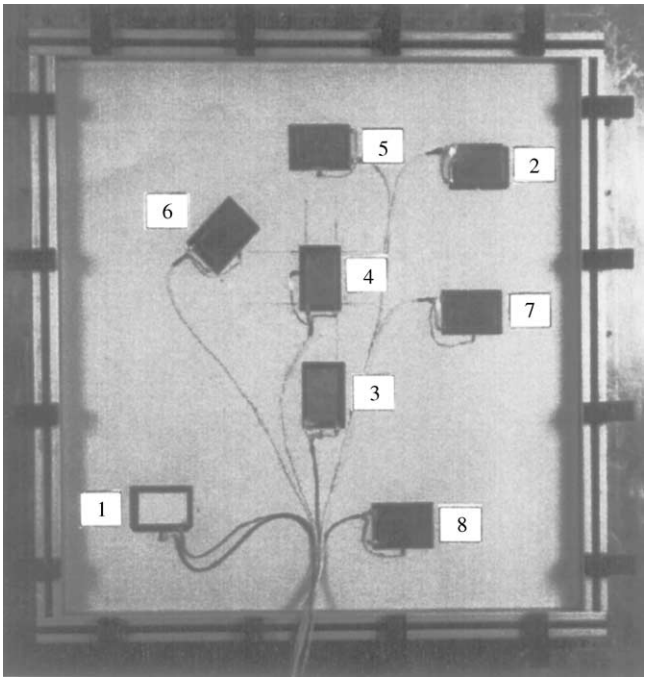

Figure 1. Final design of the equipped panel.

Dynamic shakers were used for comparison purposes, as they are usual laboratory vibration exciters.

The sensors were of three different types:

(1) eight PVDF (polyvinylidene fluoride) patches were collocated with the corresponding PZT actuators, on the other side of the panel;
(2) two sets of accelerometers were used, three of which were collocated with the secondary shakers, and eight others were placed either at random on the plate, or on the PVDF patches;
(3) finally, three microphones were located in the receiving room, 0·1 m away from the panel, and used as error sensors for feedforward experiments;

In all the cases, the pressure field radiated by the plate was measured by a microphone moved in a plane 1·2 m in length and 0·36 m in height, located 1 m away from the panel. When a single figure (in dB) is given for pressure reductions, it refers to the sum of the squared pressure amplitudes over the measured area, and is often termed as "global" reduction. A positive value indicates a pressure reduction, and a negative value a pressure increase.

3. THEORETICAL ASPECTS

3.1. MODELLING AND IDENTIFICATION ISSUES

Finite element calculations were first performed using NASTRAN software on the panel with free boundary conditions applied on its four sides. The results were compared to a first set of experimental measurements. This first step allowed an updating of the material

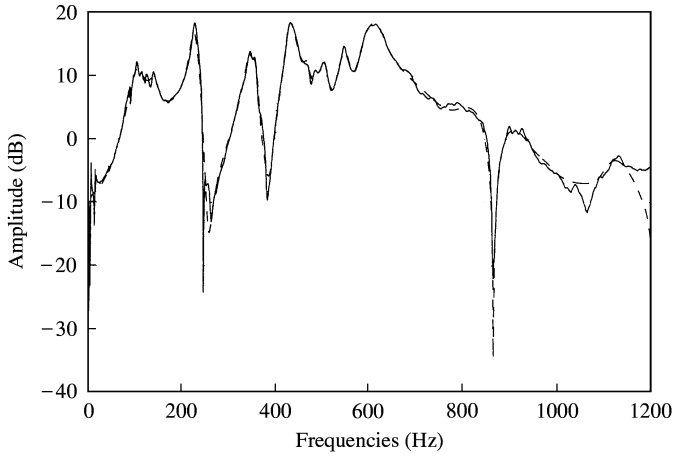

Figure 2. Transfer function between shaker and PVDF #1 sensor.

coefficients (particularly damping ratios), which are not always very well known for honeycomb panels. In a second step, the same type of calculations were carried out with boundary conditions representing the clamping devices. It is worth mentioning that these devices added some damping to the structure. The latter results provided baseline data for optimizing actuator locations.

The method followed for the optimal positioning of the actuators is summarized here. The model issued from finite element calculation was cast in the following state-space formulation:

$$\dot{X} = AX + Bu, \qquad y = CX + Du. \tag{1}$$

In this equation, X is the state variable vector, u the vector of control inputs, and y the vector of sensor outputs. The input and output influence matrices are B and C, and A is the system matrix. Due to the collocation between actuators and sensors, it is equivalent to optimize the position of the former or that of the latter. One way of maximizing the observability of the panel modes is to maximize the value of the cost function trace $(C^{\top}C)$. The reason as to why this is a measure of the system observability is because the term $C^{\top}C$ is present in the observability gramian $G = \int_0^{\infty} \mathrm{e}^{At} C^{\top} C \mathrm{e}^{A^{\top}t}\,\mathrm{d}t$. Since the sensors and actuators do not change significantly the structure poles, matrix A can be considered to be constant during the optimization process.

However, it turns out to be very difficult to find a reliable way of placing all sensors (or actuators) simultaneously. On the other hand, positioning one sensor at a time gives the interesting flexibility of changing for each sensor the state variable set on which the observability measure is based. Typically, the first sensor is placed so as to maximize the observability of all modes, then the second is placed in order to sense the modes that were not very well sensed by the first sensor, and so on ....

In a second step, data acquisitions were carried out on the equipped panel: impulse responses measured by accelerometers were used for modal analysis investigations, because this measurement method allows a large number of excitation points (impact hammer locations) to be used. For system identification (see equation (1)), transfer functions between piezoelectric actuators (or shaker) and sensors were employed. An example of such a transfer function is shown in Figure 2.

The method selected for system identification was Eigensystem Realization Algorithm and Observer/Kalman filter Identification (ERA-OKID) [15]. This identification method builds a discrete state-space representation of the system from its impulse responses, or from the impulse responses of a suitable observer. This method is known to be difficult to apply to very lightly damped structures, and thus appeared more successful in the present case, where structural damping was significant. The state-space representation issued from the ERA-OKID procedure served as a basis for feedback control synthesis and optimization.

An analytical model was also used to calculate an approximation of the dynamic response and the radiated pressure field of the orthotropic sandwich panel, with and without control, at a lower computational cost [16]. This calculation was made for different locations of microphones as error sensors and shakers as secondary actuators. The mechanical characteristics and especially the loss factors were updated through multi-reference modal analysis. The measurement of the radiated pressure field validated the free-space Green function assumption used for the corresponding calculations.

Because of the complexity of this damped structure, the analytical model, as well as the FEM model, are only helpful guides for sensor and actuator placement.

3.2. FEEDFORWARD CONTROL

3.2.1. *Controller design*

The algorithm selected for the experiments is the well-known filtered-x least mean squares (LMS) algorithm [17]. This is a simple minimization procedure which belongs to the class of stochastic gradient algorithms. A very good presentation can be found in reference [17] or [10], but the method is summarized here for the sake of completeness.

The starting point is the block diagram shown in Figure 3. Block G represents the dynamic system, with control input u and output s. Here, u is the input signal fed to the secondary actuator (shaker or piezoelectric patch). A disturbance signal d is added to the system output, and the error signal is denoted $e = s + d$. x is a reference signal, closely correlated with the disturbance d. The goal is to determine the control filter W so that the system output s cancels the disturbance d, thus minimizing the error signal e.

Under the assumption that G and W are either time-invariant or slowly varying, it is possible to permute the corresponding blocks, resulting in the block diagram shown in Figure 4. A new signal r appears, called the filtered reference. The problem can then be recast into that of optimally filtering this filtered reference with the objective of minimizing the expected value J of the error signal e squared. An identification of block G is required prior to control. It can be achieved for example by random excitation of the secondary actuators and a decorrelation process.

A number of algorithms can then be applied to compute the W filter coefficients. If only finite impulse response (FIR) filters are employed for G and W, the LMS algorithm may be used. It is a simple iterative procedure that can be written as

$$W_i(n+1) = W_i(n) - 2\mu e(n) r(n-i). \tag{2}$$

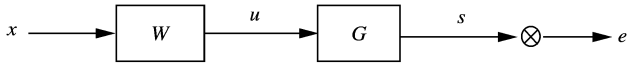

Figure 3. Block diagram of feedforward control.

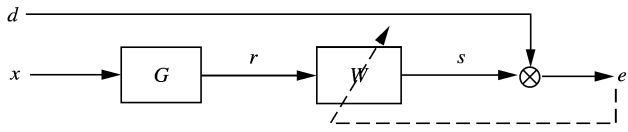

Figure 4. Block diagram of LMS algorithm.

In the preceding expression, $W_i(n)$ is the ith coefficient of filter W at time step n, and μ is a convergence coefficient. In fact, $2e(n)r(n-i)$ is an approximation of the gradient of the cost function J with respect to the filter coefficient W_i.

This algorithm or its variants are by far the most widely used in the active control community. Its convergence and stability properties are very well known [18], and it is very easy to implement in real time.

3.2.2. *Performance analysis*

The filter lengths are theoretically selected according to the tested frequency band, the sampling frequency and the frequency resolution. In practice, the controller is implemented in real time on a digital signal processor (DSP). The computation time, which depends on the DSP performance, rapidly increases with the filter size. As this processing time must remain shorter than the sampling period, the filter lengths are in fact bounded by some practical limit.

Moreover, the rate of convergence depends on the frequency band, while the convergence coefficient μ was assumed to be constant in equation (2). In practice, a given convergence coefficient can cause a divergence at some frequency while being too low to guarantee a rapid convergence at another frequency. For this reason, the LMS algorithm has mainly been used for sinusoidal perturbations or narrowband excitations.

Another solution can be to perform the control in the frequency domain and to use a particular convergence coefficient in each frequency band.

In the present case, several features make it possible to extend the field of application of this algorithm.

(1) The high structural damping leads to smooth transfer functions between actuators and sensors in the modal domain. This results in shorter FIR filters than in the case of lightly damped materials.
(2) The collocated nature of the actuators and sensors leads to impulse responses that do not include propagation delays.
(3) The use of single input single output (SISO) algorithms, instead of a multi-input multi-output (MIMO) algorithm reduces the computation time. Identification is also improved in this case, because of better coherence between collocated input and output signals.

The real-time calculations were performed on a TMS320C31 DSP. Its current capabilities allow the use of three sensors/actuators and one reference input. In the practical implementations of the present work, the sampling frequency varied between 2700 and 3900 Hz. The length of the identified FIR filters generating the filtered reference was 10–45, and that of the adaptive control filters (also FIR) was 9–15. A MIMO loop was used in the case of pure tone excitations, and 3 SISO loops for broadband excitations.

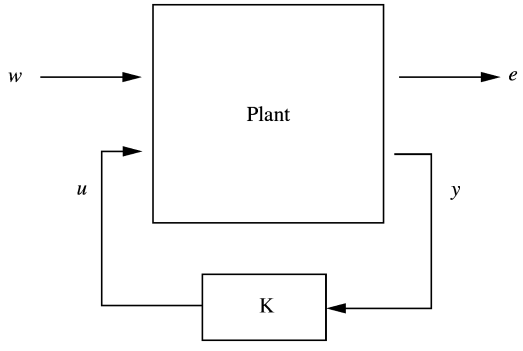

Figure 5. Block diagram of the standard feedback problem.

3.3. FEEDBACK CONTROL

3.3.1. *Controller design*

The model resulting from system identification (see section 3.1) is a suitable basis for controller design. It was used to optimize the filter coefficients in the framework of the so-called Positive Position Feedback (PPF) design methodology [19], described in the following paragraphs.

Let us refer to the standard feedback problem, illustrated by the block diagram of Figure 5. The disturbance input w corresponds to the primary shaker force, and the error signal e is the output to be minimized. In our case, this performance metric is provided by two means: the signal of eight accelerometers placed on the panel and, of course, the pressure field measured by a moving microphone in the receiving room, 1 m away from the panel. The sensor out-put (y) and control input (u) signals come from collocated pairs: either PVDF patches versus PZT patches, or three accelerometers versus three secondary shakers. In the experiment, independent SISO loops were implemented.

The PPF design methodology takes advantage of this collocated nature of the sensor and actuator sets, which imparts the following properties to the system: the phase of the collocated transfer functions varies between 0 and -180°; the system poles and zeros alternate along the imaginary axis.

The root locus in Figure 6 is relative to a discrete SISO model fitted to the collocated transfer function between one PZT patch and the collocated PVDF patch, using the ERA-OKID method outlined in section 3.1. The continuous to discrete transform maps the imaginary axis onto the unit circle, and therefore the poles ($\times$'s) and zeros ($\bigcirc$'s) of the discrete model alternate along the unit circle in this representation.

Applied to a positive system, a positive feedback controller makes the closed loop unconditionally stable [20]. In our case, the natural feedback strategy is Positive Position Feedback, whereby sensor output signals are fed back to the actuators through a second order filter (or a number thereof). The time-domain equations read as follows.

System dynamics:

$$\mathbf{M}\ddot{q}(t) + \mathbf{C}\dot{q}(t) + \mathbf{K}q(t) = bu(t) + b_f f(t), \quad y(t) = cq(t) + du(t). \tag{3}$$

Here, q refers to the generalized co-ordinates. $\mathbf{M}$, $\mathbf{C}$, $\mathbf{K}$ are the mass, damping and stiffness matrices respectively. u is the control input, y the measured output, and f an

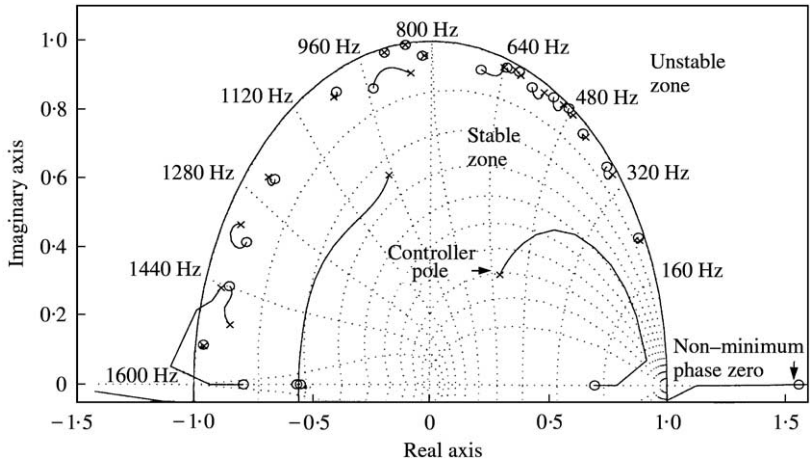

Figure 6. Root locus in discrete time of one sensor/actuator pair.

exogeneous force input. b, c, and b_f are the corresponding influence matrices. d is the feedthrough term.

Controller dynamics:

$$\ddot{u}(t) + 2\xi\omega_o\dot{u}(t) + \omega_o^2 u(t) = g\omega_o^2 y(t). \tag{4}$$

g denotes the feedback gain, and ω_o and ξ define the filter cut-off frequency and damping ratio. In the experiment, a critical damping ratio ($\xi = 0{\cdot}7$) was used. The filter cut-off frequency ω_o and the gain g are tuned through numerical simulations based on Black diagrams to guarantee sufficient gain and phase margins.

Closed-loop equation (Laplace domain):

$$\left[s^2\mathbf{M} + s\mathbf{C} + \mathbf{K} - \omega_o^2 \frac{bgc}{s^2 + 2\xi\omega_o s + \omega_o^2(1 - gd)}\right] q(s) = b_f f(s). \tag{5}$$

The effect of control is to change the system poles, as usual in feedback. Here, this effect is mainly focused on the system stiffness in the lower frequency range, where the control term in equation (5) reduces to the constant $bgc/(1 - gd)$. It then tends to increase the system damping around the filter cut-off frequency. More details are to be found in reference [19].

Another often mentioned low-order control strategy is velocity feedback, where the velocity output $y_v(t) = c_v\dot{q}(t)$, is used and where the control law is simply $u(t) = g_v y(t)$. However, PPF control seems to be more appropriate here, because of the following advantages over velocity feedback. First, a velocity measurement is not easily implemented and tends to amplify high frequency components. Secondly, velocity feedback involves a constant feedback gain, which lacks sufficient roll-off at high frequencies.

3.3.2. *Performance analysis*

The root locus corresponding to one sensor/actuator pair, shown in Figure 6, is a good illustration of the feedback effect, using PPF control. It represents the system poles (depicted by $\times$'s) in their open-loop position, and the trajectories of the closed-loop poles as functions of the feedback gain. These trajectories end in the positions of the system zeros

(depicted by ○'s). The effect of the control law on the pole stiffnesses and damping is visible, through the shape of those trajectories.

This root-locus also highlights two potential problems: first, conditioning filters can introduce non-minimum phase zeros (i.e., located outside the unit circle) in the open loop, such as the one plotted at the right end of the graph. Since the closed-loop pole trajectories end in the corresponding zeros, this problem can lead to low-frequency destabilization of the closed loop. Indeed, one of the pole trajectories does end in the non-minimum phase zero (see Figure 6).

Secondly, power amplifiers usually have a low-pass filter transfer function that adds some delay in the open loop, setting a limit on the positivity of the combined system. This feature has an effect on the pole trajectories, which are supposed to stay within the unit circle under the assumption of positivity, thus providing the stability guarantee. This is obviously not the case for the trajectory originating in the 1440 Hz pole in Figure 6. From practical point of view, these side effects limit the gain that can be applied to the controller.

It is clear that such a control approach has a number of advantages and drawbacks, as follows.

(1) It is robust to changes in the structure dynamics, due to the smooth shape of the controller transfer function.
(2) It is simple to implement, and does not require huge real-time computing capabilities.

On the other hand:

(1) It does not allow the control authority to be focused on particular combinations of modes. This possibility is available when using the well-known LQG control synthesis methodology. In this case, a cost function is minimized, and this cost function can be defined taking advantage of radiation filter outputs [21–23, 10] or other mode combinations suited to effectively control the noise radiation of the panel. However, the use of LQG control methodology has very limited robustness properties that prevent its application to real structures vibrating in environments that are not well known.
(2) Controller performance is closely related to the location of the actuators and sensors, without much flexibility once they have been determined.

The following experimental results show that the positive position feedback approach taken in this paper is still a good compromise between controller simplicity and efficiency.

3.4. FEEDFORWARD/FEEDBACK COMPARISON

Comparison of the two approaches requires the use of a common language. A recent article [24] provides some insight into the relationship between feedback and feedforward control approaches, based on the same general formalism. Referring to Figure 5, the different transfer functions connecting system inputs and outputs are termed: *performance path* between w and e, *control path* between u and y, *reference path* between w and y and *secondary path* between u and e.

Feedforward control designers are familiar with the *reference* and *secondary* paths, since they do not take advantage of a direct measurement y. The disturbance signal d discussed in section 3.2 is equivalent to the signal w "seen" by the output, and hence filtered by the structural/acoustic system. The performance of the LMS algorithm is directly proportional to the correlation between x and d. Information on the system dynamics is contained in the *secondary path* transfer function, corresponding to block G in Figure 3. Performance

of this kind of feedforward controllers for broadband excitations can therefore be limited by a lower correlation between the two signals x and d than for a periodic perturbation.

In contrast, feedback control designers do not have a *reference path*, and have to make do with the measured output y. Information on the system dynamics is modelled either through pole-zero transfer functions or through a state-space representation, and is relative to the *control path*. As an example, LQG design methodology takes the error signal e into account through a cost function, and assumes the disturbance input to be Gaussian.

4. FEEDFORWARD CONTROL EXPERIMENTS

4.1. PURE TONE EXCITATIONS

The panel was equipped with one or two miniature shakers excited successively at 242 and 554 Hz, frequencies identified as very close to the resonant frequencies of the (2–1) and (2–3) modes (an (i–j) mode has i antinodes in the horizontal direction and j antinodes in the vertical direction). Microphones located 0·1 m away from the panel were used as error sensors.

The radiated field is representative of many modes, because of the high structural damping (between 1 and 10%). Moreover, a theoretical analysis [16] shows that the pressure distribution over a plane parallel to the panel is due to multi-modal interactions and varies strongly according to the distance from the panel to the plane. This phenomenon is typical of nearfield acoustic radiation, and will influence the location of secondary actuators.

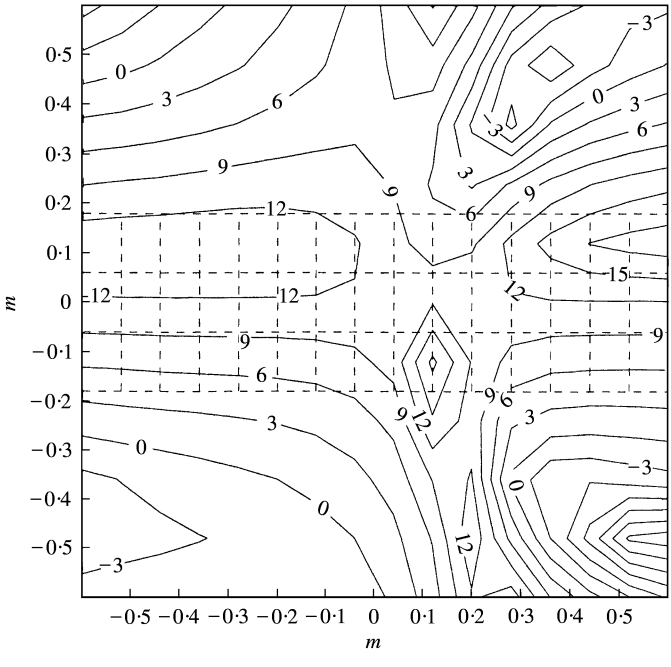

Figure 7. Theoretical prediction of the pressure reductions. The grid indicates the actual measured surface. Primary excitation: pure tone at 554 Hz.

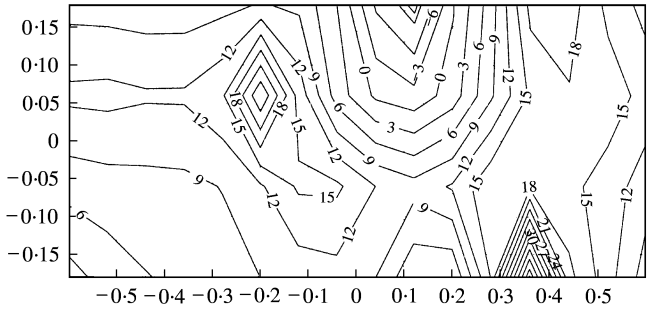

Figure 8. Feedforward control at 554 Hz, mics as error sens., shakers as second. act. Experimentally measured pressure reductions distribution (dB).

TABLE 1

Feedforward control performance under sinusoidal excitation

Frequency (Hz)	Secondary actuators/ error sensors	Global reduction at error sensors (dB)	Max. reduction on meas. plane (dB)	Global reduction on meas. plane (dB)
242	Shakers/microphones	20·3	9	4·6
554	Shakers/microphones	11	20	9·6
242	PZT/PVDF	40·5	18	3·6
554	PZT/PVDF	30	26	4·5

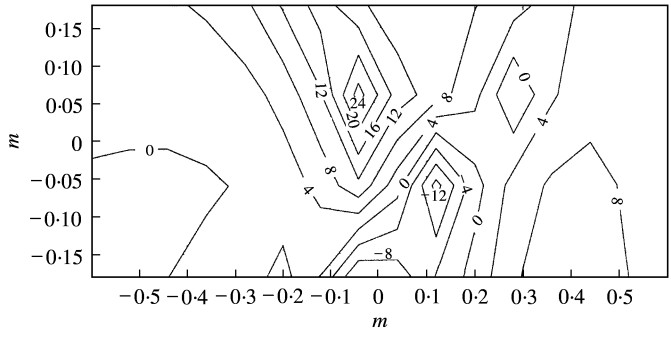

Figure 9. Feedforward control at 554 Hz, PVDF as error sens., PZT as second. act. Experimentally measured pressure reductions distribution (dB).

Figure 7 shows the theoretical reduction with a MIMO algorithm in a $1{\cdot}2 \times 1{\cdot}2\,m^2$ plane that includes the measurement plane. The simulation is representative of the experiment (Figure 8) and predicts a global pressure reduction of 10·4 dB. The best experimental results with microphones and shakers or collocated PVDF/PZT patches as error sensors and secondary actuators are shown in Table 1. Global pressure reductions are generally higher with microphones than with PVDF, and also better spread on the measurement plane (see e.g., Figures 8 and 9). One can see that the acoustic field level is increased in the area of the pressure nodes of the primary field.

TABLE 2

Voltage reductions of PVDF films (dB) under broadband excitation

Frequency band (Hz)	Film 4	Film 5	Film 7	Films 4 + 5 + 7	Films 2–8
85–285	5·6	9	4·7	5·3	1·7
500–700	12·4	15·6	9·2	12·8	5·3
400–800	8·7	8·1	3·9	6·9	2·9

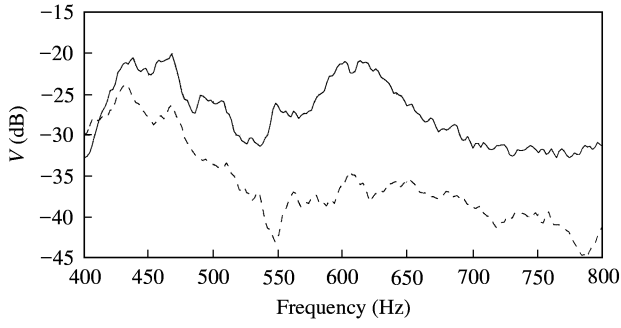

Figure 10. Feedforward control on 400–800 Hz, PVDF as error sens., PZT as second. act. Sum of experimentally measured voltages of the 3 error sensors (PVDF 4, 5 and 7). —— control off; – – – control on.

4.2. BROADBAND EXCITATIONS

The reduction of a broadband excitation required longer filters and a higher number of actuators and error sensors, which was not possible with a MIMO algorithm due to DSP limitations. This problem was solved by using as many SISO algorithms in parallel as there were collocated PVDF/PZT patches. In this case, in contrast to a MIMO algorithm, each sensor measured a disturbance signal d whose value decreased during convergence. In effect, d took the contribution of the non-collocated secondary actuators into account. Nevertheless, this variation was not detrimental to the stability and the control performance (error signal reduction).

Table 2 shows the voltage reductions obtained on the PVDF films. Films 4, 5 and 7 are the error sensors. These results are presented for several frequency bands of excitation with SISO algorithms. Figure 10 shows that reductions were achieved on the entire frequency band (400–800 Hz in this case) at the error sensors. However, the pressure is only reduced on part of the measured area (Figure 11).

4.3. PRELIMINARY CONCLUSIONS

The above-mentioned feedforward experiments show that, for single frequency primary excitations, it may be sufficient to optimize the location of a few actuators and error sensors (distributed or not) to obtain significant pressure reductions of large surfaces. Because of the acoustic radiation of resonant modes, it is more efficient to use microphones as error sensors than PVDF patches. Nevertheless, when the number of damped modes increases, pressure reductions are relatively local (presence of modal overlap). Finally, there do not

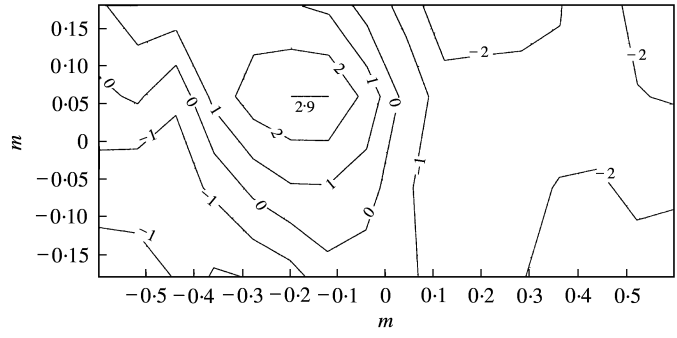

Figure 11. Feedforward control on 400–800 Hz, PVDF as error sens., PZT as second. act. Experimentally measured pressure reductions distribution averaged on 400–800 Hz (dB).

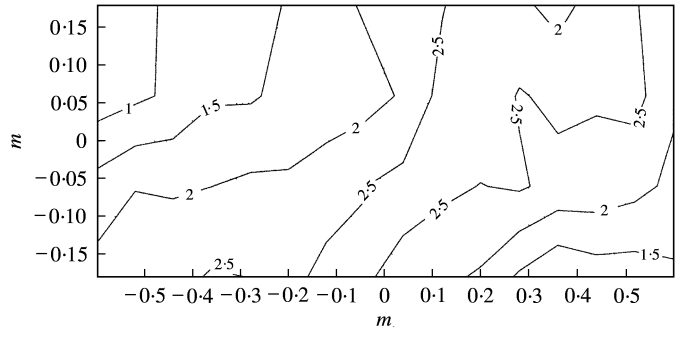

Figure 12. Feedback control on 0–800 Hz, shakers as secondary actuators. Experimentally measured pressure reductions distribution averaged on 80–400 Hz (dB).

seem to be significant differences in efficiency between the two types of actuators (minishakers and PZT patches).

For broadband primary excitations, use of SISO algorithms with collocated PVDF/PZT patches represents an interesting solution which allows an increase in the sampling frequency and filter lengths. The results reported herein show significant reductions in the 400–800 Hz wide frequency band, in agreement with the remarks of section 3.2.2: the high structural damping makes the system transfer functions smooth, more accurately modelled by rather short FIR filters than with lightly damped materials.

5. FEEDBACK CONTROL EXPERIMENTS

Feedback control experiments were conducted only for broadband primary excitations. The design strategy described above (see section 3.3) led to one filter characteristic per sensor/actuator pair. In the experiments, piezoelectric elements 3 and 4 (see Figure 1) were combined in the following way: the same input signal was fed to both actuators and the output signal was the sum of the two sensor voltages. Actuator 1 was not used, because symmetrically located actuator 2 was sufficient. There were therefore six independent control channels in all, and of course only three in the accelerometer/shaker configuration.

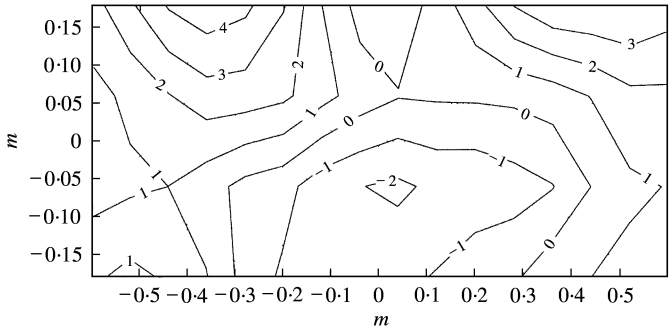

Figure 13. Feedback control on 0–800 Hz, shakers as secondary actuators. Experimentally measured pressure reductions distribution averaged on 400–800 Hz (dB).

5.1. ACCELEROMETERS/SHAKERS

The first experimental example is relative to the use of three shakers as secondary forces and the corresponding collocated accelerometers as sensors. Three independent SISO loops were implemented. Controllers were three low pass filters with different cut-off frequencies (200, 300, 400 Hz) and critical damping ratio $\xi = 0{\cdot}7$. Results are plotted in two separate frequency ranges (Figures 12 and 13), even though the control law and primary excitation spectrum were unique (0–800 Hz). The pressure reduction in the first frequency range is global on the entire measured area, whereas, for the second frequency band, the pressure increases in one area. Even if the reduction levels are moderate, there is a real potential for noise attenuation on a wide frequency band.

5.2. PVDF/PZT PATCHES

The experiment involving PVDF patches as sensors and PZT patches as actuators is more successful and speaks for the use of distributed sensors and actuators. In that case, six independent SISO loops were implemented using the patches 2, 3 + 4, 5, 6, 7 and 8. Controllers were low pass filters with respective cut-off frequencies 500, 500, 300, 600, 300 and 300 Hz.

Figure 14 shows the sum of eight squared accelerometer outputs (i.e., not used in the control loop) over the entire frequency band. The attenuation is quite significant on the entire bandwidth, and amounts to 10 dB in some places.

In order to allow a direct comparison with the previous case, pressure reduction distributions are also presented, averaged on the same two frequency bands (Figures 15(a) and 15(b)).

The reductions obtained in the lower frequency band are slightly better than those obtained using point actuators, with values ranging from 2·5 to 5 dB. This behavior is probably linked to the dissipative nature of the composite panel, which makes point actuators less likely to induce global displacement field in the panel. Again, the reduction is more questionable in the upper frequency band, but also more successful than in the previous case.

A concise presentation of the feedback control results is given in Table 3. The actuators 3 + 4, 6 and 8 were efficient only in the 80–250 Hz frequency range. This leads us to consider that the result obtained in the frequency band 250–800 Hz (Figure 15(b)) is relative to an actual 3 channel configuration.

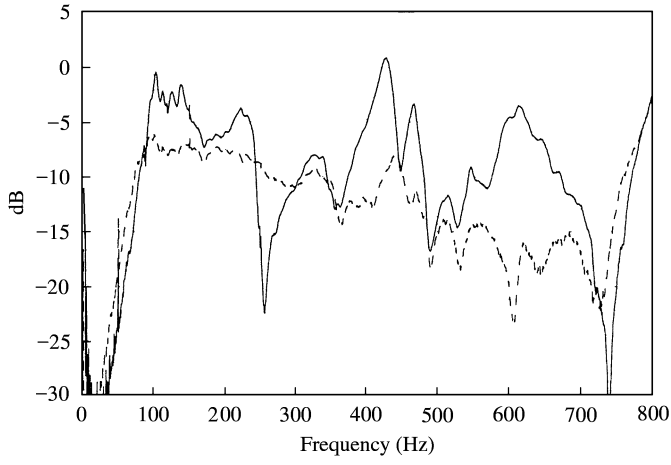

Figure 14. Sum of the measured autospectra of the independent accelerometers located on the panel, PZT as actuators. —— open loop, – – – closed loop.

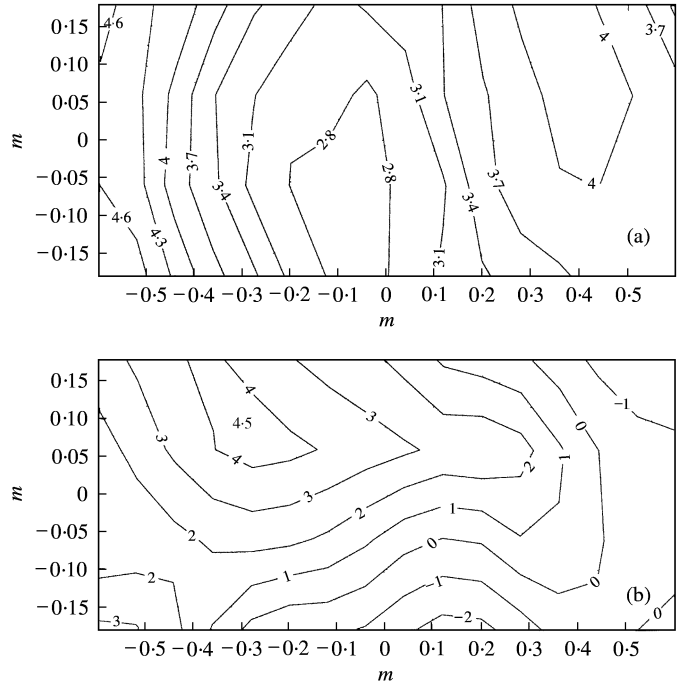

Figure 15. Feedback control on 0–800 Hz, PZT as secondary actuators. Pressure reductions distributions (dB) averaged on (a) 80–400 Hz; (b) 400–800 Hz.

6. EXPERIMENTAL COMPARISON

In the present work, comparisons between the two approaches are limited to the broadband case. The reasons for this choice are that: (1) broadband control is not as well documented in the literature as sinusoidal control, and (2) fixed (as opposed to adaptive)

TABLE 3

Minimum and maximum pressure reductions averaged over the indicated frequency band, under broadband

Frequency band (Hz)	Actuator	Feedback		Feedforward	
		Min. red.	Max. red.	Min. red.	Max. red.
85–400	Shaker	1	2·5		
400–800	Shaker	− 2	4		
80–400	PZT	2·8	4·6		
400–800	PZT	− 2	4·5	− 2	2·9

feedback control performances do not directly depend on the frequency content of the perturbation. A given controller therefore achieves at least the same performance in narrowband as in a broader frequency range.

The comparison is based on the results shown in Figures 11 and 15(b). Both results refer to the same number of actuators (see section 5.2 for details), the same frequency band of analysis (400–800 Hz), and slightly different control configurations: feedback control is applied with primary excitation to the whole frequency band (0–800 Hz), whereas feedforward control is relative to primary excitation on the limited 400–800 Hz band.

Turning to the actual comparison, the similarity between the pressure reduction patterns depicted in Figures 11 and 15(b) is striking, given the high complexity of the primary pressure field in this frequency range, where no less than 7 structural modes had actually been identified (among which are the very efficiently radiating odd–odd modes (1–3), (3–1), and (3–3)). The areas of high pressure reduction have the same overall shape. Both control approaches proved successful in broadband noise attenuation, even if feedback control achieved higher attenuations in this particular case (-2 to 4·5 dB reductions versus -2 to 2·9 dB), over a wider area. All pressure reduction results for broadband excitation are summarized in Table 3.

Whatever the control algorithm, in this experiment of active *noise* control, it turns out that controlling *panel vibrations* through distributed actuators and sensors results in an attenuation of the pressure field. This fact seems contradictory to some previously published studies on the topic, which point out that it is important to take the radiation efficiency of the plate modes whose frequencies lie within the frequency band of interest into account in the control law. This idea appears in many references, such as reference [22], in which the concept of "radiation modes" is introduced, but also in reference [25], where the concept of "modal restructuring" refers to the same issue, and finally in the concept of "radiation filters" [26, 11]. The common idea is that radiated noise control has to be based on an estimate of the radiated sound power, rather than on the nearfield radiated pressure.

In our case, the pressure field of interest is measured near the panel surface, and therefore the distinction between more and less efficient radiating modes is not relevant for analyzing pressure distributions. A minimum distance of 10λ, where λ is the acoustical wavelength, is usually considered as the boundary between near and far fields, if one terms as "near field" the space domain where propagative and evanescent acoustic waves coexist. In this experiment, 10λ equals 34 m at 100 Hz and 3·4 m at 1000 Hz, and therefore the pressure measurements are performed in the near field. For this reason, there is a good correlation between panel vibration reduction and nearfield pressure reduction.

It may be worth noting that the application of ASAC for interior noise in many realistic situations (helicopter cabins, airplane fuselages) involves radiating panels that can be very

close to the passengers. In those situations, it is the nearfield radiated pressure that is of importance.

7. CONCLUSIONS

This paper is focused on the application of feedforward and feedback control methodologies in an attempt to reduce noise radiation by composite structures. The test specimen was a sandwich honeycomb panel, made of a material widely used in helicopter structures.

The high structural damping inherent to this type of material had important consequences: finite element modelling and modal analysis were much more complicated than for metallic panels, and the initial damping level was comparable to that of a controlled metallic plate.

The feedforward and feedback control strategies employed in the present study were presented and compared on the same test specimen, using the same measurement apparatus in the same lab environment. In addition, several sensor/actuator arrangements were evaluated. The frequency band for broadband excitation was 0–800 Hz.

Feedforward control was applied for pure tone excitations, where it was demonstrated that the choice of proper actuators and sensors can lead to efficient radiated pressure reduction. Better results were obtained when microphones were used as error sénsors. Significant pressure attenuations were measured: up to 10 dB averaged over an extended measurement area.

For wideband excitations, this control approach was also effective, due to the fact that the structure "smooth" transfer functions could be modelled by short FIR filters. It nevertheless required significant real-time computing capabilities. Up to 3 dB pressure reductions were observed in the measurement area, on the 400–800 Hz frequency band.

Feedback control was applied for broadband excitations only, and simple analog SISO loops based on the distributed PVDF sensors-PZT actuators led to a good pressure attenuation, extended over the range of frequencies as well as over the entire measurement area. No pressure measurements were used in the control loop. Pressure reductions amounted to 4·6 dB on the lower frequency range (80–400 Hz) with no pressure increase and to the same value on the upper frequency band (400–800 Hz).

It was also shown that for nearfield pressure reduction, it may not be necessary to use the concepts of radiation filters or radiation modes, since the cost function is actually this nearfield pressure, and not an estimate of the total radiated sound power, more representative of farfield radiation.

ACKNOWLEDGMENTS

The authors gratefully acknowledge the continuing financial support of DGA for this study.

REFERENCES

1. F. FAHY 1987 *Sound and Structural Vibration*. New York: Academic Press.
2. T. T. HYDE, editor 2000 *Smart Structures and Materials Conference*, Vol. 3989.
3. F. SIMON and S. PAUZIN 1995 *Proceedings of Euro Noise* '95, *Lyon*, *France*. Sound transmission loss model of orthotropic sandwich panels.

4. C. R. FULLER 1990 *Journal of Sound and Vibration* **136**, 1–15. Active control of sound transmission/radiation from elastic plates by vibration inputs. I. Analysis.
5. V. L. METCALF, C. R. FULLER, R. J. SILCOX and D. E. BROWN 1992 *Journal of Sound and Vibration* **153**, 387–402. Active control of sound transmission/radiation from elastic plates by vibration inputs. II. Experiments.
6. J. PAN, S. D. SNYDER, C. H. HANSEN and C. R. FULLER 1992 *Journal of the Acoustical Society of America* **91**, 2056–2066. Active control of far field sound radiated by a rectangular panel. A general analysis.
7. B. PETITJEAN and I. LEGRAIN 1996 *Journal of Structural Control*. **3**, 111–127. Feedback controllers for active vibration suppression.
8. B. PETITJEAN and I. LEGRAIN 1994 *Second European Conference on Smart Structures and Materials Vol. SPIE* 2361, *Glasgow*. Feedback controllers for broadband active noise control.
9. S. J. ELLIOT and G. HORVÀTH, editors 1997 *Proceedings of Active* '97, *International Symposium on Active Control of Sound and Vibration*. Budapest: Publishing Company of Technical University of Budapest.
10. C. R. FULLER, S. J. ELLIOT and P. A. NELSON 1996 *Active Control of Vibration*. New York: Academic Press.
11. R. L. CLARK and K. D. FRAMPTON 1999 *Journal of the Aoustical Society of America* **105**, 743–754.
12. J. R. F. ARRUDA, F. J. O. MOREIRA and A. K. A. PEREIRA 1997 *Proceedings of Active* '97, *Budapest*, *Hungary*, 75–92. Comparing feedback vibration control and feedforward power-flow-based control strategies using a simple plate example.
13. S. J. ELLIOT and B. RAFAELY 1997 *Proceedings of Active* '97, *Budapest*, *Hungary*, 771–787. Frequency-domain adaptation of feedforward and feedback controllers.
14. C. BAO and J. PAN 1997 *Journal of the Acoustical Society of America* **102**, 1664–1670. Experimental study of different approaches for active control of sound transmission through double walls.
15. JER-NAN JUANG 1994 *Applied System Identification*. Englewood Cliffs, NJ: Prentice-Hall.
16. F. SIMON and S. PAUZIN 1997 *Proceedings of Active* '97, *Budapest*, *Hungary*, 1035–1048. Simulation of an active vibration control procedure: simulation/experiment comparison.
17. S. J. ELLIOT, I. M. STOTHERS and P. A. NELSON 1987 *IEEE Transactions on Acoustics, Speech, and Signal Processing* **ASSP-35**, 547–564. A multiple error LMS algorithm and its application to the active control of sound and vibration.
18. S. HAYKIN 1991 *Adaptive Filter Theory*. Englewood Cliffs, NJ: Prentice-Hall.
19. J. L. FANSON and T. K. CAUGHEY 1990 *American Institute of Aeronautics and Astronautics Journal* **28**, 717–724. Positive position feedback for large space structures.
20. R. J. BENHABIB and R. P. IWENS 1981 *American Institute of Aeronautics and Astronautics Journal of Guidance, Control and Dynamics* **4**, 487–494. Stability of large space structure control systems using positivity concepts.
21. W. T. BAUMANN, F. S. HO and H. H. ROBERTSHAW 1992 *Journal of the Acoustical Society of America* **92**, 1998–2005. Active structural acoustic control of broadband disturbances.
22. S. J. ELLIOT and M. E. JOHNSON 1993 *Journal of the Acoustical Society of America* **94**, 2194–2204. Radiation modes and the active control of sound power.
23. R. L. CLARK and D. E. COX *Journal of the Acoustical Society of America* **102**, 2747–2755. Multi-variable structural acoustic control with static compensation.
24. R. L. CLARK and D. S. BERNSTEIN 1998 *Journal of Sound and Vibration* **214**, 784–791. Hybrid control: separation in design.
25. C. R. FULLER, C. H. HANSEN and S. D. SNYDER 1991 *Journal of Sound and Vibration* **145**, 195–215. Active control of sound radiation from a vibrating rectangular panel by sound sources and vibration inputs: an experimental comparison.
26. W. T. BAUMANN, W. R. SAUNDERS and H. H. ROBERTSHAW 1991 *Journal of the Acoustical Society of America* **90**, 3202–3208. Active suppression of acoustic radiation from impulsively excited structures.